Check for updates

RESEARCH ARTICLE

A Simple Printed Circuit Board–Based Ion Funnel for Focusing Low *m/z* Ratio Ions with High Kinetic Energies at Elevated Pressure

Florian Schlottmann, [ORCID] Maria Allers, Ansgar T. Kirk, Alexander Bohnhorst, Stefan Zimmermann

Institute of Electrical Engineering and Measurement Technology, Department of Sensors and Measurement Technology, Leibniz University Hannover, Appelstr. 9A, Hannover, 30167, Germany
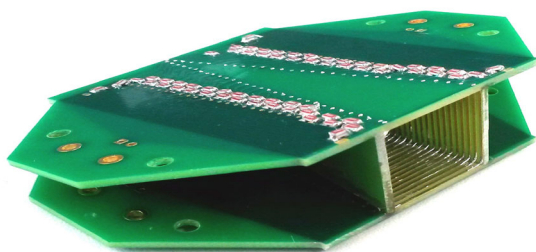
Abstract. Ion funnels are one of the key components for transferring ions from higher pressure into the vacuum. Typically, ion funnels are constructed of several different plate ring electrodes with a decreasing inner diameter where radio frequency (RF) voltages and electric DC fields are applied to the electrodes to focus and transport ion clouds. In this work, we developed and investigated a simple and low-cost ion funnel design that is based on standard printed circuit boards (PCB) with integrated planar electrodes including the signal distribution network. This ion funnel is capable of withstanding high electric fields with superimposed RF voltages due to its buried capacitors. To evaluate the ion focusing efficiency of the ion funnel, we simulated the movement of ions inside this funnel and experimentally evaluated the ion transfer. Our simulations show that a rectangular ion funnel like the PCB ion funnel has similar performance compared with conventional stacked ring funnels. Due to the hundredfold lower parasitic capacitance between the planar electrodes compared with conventional ion funnels, high RF voltage amplitudes up to 195 V and reduced electric DC field strengths up to 100 Td can be reached at a frequency of about 5 MHz. Thus, the funnel is appropriate to focus light ions at elevated pressures up to 20 mbar.

Keywords: Electrodynamic ion funnel, Printed circuit board, Rectangular ion funnel, Low *m/z* ratio, Low parasitic capacitance

Introduction

Proton-transfer-reaction drift tubes in PTR-MS [1, 2] or the recently introduced high kinetic energy ion mobility spectrometers (HiKE-IMS) [3–5] are operated at reduced electric field strengths up to 120 Td (HiKE-IMS) or 140 Td (PTR-MS) at pressures between 2 mbar (PTR-MS) [6–8] and 20 mbar (HiKE-IMS) [3–5]. These high reduced electric field strengths result in average kinetic ion energies up to 0.2 eV, which are fairly high compared with IMS typically operated at ambient pressure with reduced electric field strengths below 10 Td [9].

Due to the high number of ion-neutral collisions, the gas phase ion-molecule chemistry in the PTR drift tube or the HiKE-IMS is based on complex cluster chemistry being affected by temperature, pressure, and reduced electric field strength. To investigate the gas phase ion-molecule reactions in these devices, a mass spectrometer (MS) needs to be coupled with an effective ion transfer into the MS. Aiming for the analysis of cluster sizes, an "energy neutral" transfer would be preferable, so that the kinetic ion energy is not affected by the transfer.

Typically, starting in the mbar pressure range, various concepts are possible for the transfer of ions in a subsequent pressure stage. For example, a simple pinhole can be placed between the pressure stages [10, 11]. Using a pinhole, ions would just experience a defined energy input from electric DC fields. However, in the absence of a focusing element, ion losses would be rather high. By

Correspondence to: Florian Schlottmann; *e-mail:* schlottmann@geml.uni–hannover.de

extending the pinhole geometry with an additional focusing electrode resulting in a so-called tube lens [12, 13], ion losses can be decreased. However, ions gain additional energy in the focusing field leading to possible declustering processes.

In the last two decades [14, 15], ion funnels have become widely used as transfer elements in mass spectrometry. Ion funnels consist of a series of electrodes with progressively reducing aperture sizes. An electric DC field drives the ions axially through the ion funnel towards the exit aperture. In addition, superimposed RF potentials of opposite polarity are applied to adjacent electrodes. The RF field generates a strong repulsive effective potential near the surface of each electrode, which, coupled with the progressively decreasing aperture size, focusses the ions radially. This focusing effect significantly increases the ion flux through the exit aperture [16, 17]. In contrast, an ion funnel allows for two different operating modes: (a) having zero RF voltage, the ion funnel serves as a simple pinhole suffering from ion loss but providing a defined energy input controlled by the electric DC field and (b) with increasing RF voltage, ion losses decrease, but energy input increases. Therefore, an ion funnel enables switching between those two operating modes without modifying the experimental setup. Due to this flexibility, we consider the ion funnel to be the most appropriate transfer element for HiKE-IMS-MS that is meant for investigating the ion chemistry in the HiKE-IMS. Hence, the aim of this work is to design an ion funnel for this particular application. Typically, ion funnels are applied in mass spectrometers used in life sciences [18, 19] or atmospheric chemistry [20]. They work in a pressure range from 1.3 to 13 mbar [21, 22]. At these pressures, they show efficient focusing for large molecules with molecular weights higher than 500 u [19, 22, 23] using frequencies between 560 kHz [18] and 3 MHz [22] and RF voltage amplitudes up to 200 V (zero-to-peak) [22] as well as reduced electric field strengths between 0 and 10 Td [24, 25].

For a HiKE-IMS-MS, aiming for better understanding of the ion chemistry in HiKE-IMS including cluster formation, an "energy neutral" ion transfer would be ideal. When the ion funnel has zero RF voltage and serves as a simple pinhole, the energy input is controlled by the electric DC field. Therefore, the ion funnel should be able to operate at the same reduced electric field strength as the HiKE-IMS, thus at reduced electric DC field strength up to 120 Td. The resulting electric field strength for 120 Td at 20 mbar and 20 °C is about 60 V/mm and rather high for conventional ion funnels. Hence, the ion funnel has to withstand both high DC voltages as well as superimposed RF voltages. Furthermore, for efficient ion focusing at elevated pressures up to 20 mbar like in the HiKE-IMS, the operating parameters of the ion funnel need to be adjusted.

The maximum effective potential $V_{\max}$ generated by the RF field in the ion funnel is estimated using Eq. (1) [26].

$$V_{\max} = \frac{q \bullet V_{\mathrm{RF}}^2}{4 \bullet m \bullet \omega^2 \bullet \left(\frac{d}{\pi}\right)^2} \tag{1}$$

Here, ω is the angular frequency, V_{RF} is the RF voltage amplitude, m is the molecular mass of the ion, q is the charge of

the ion, and d is the center-to-center distance between the electrodes. However, this equation neglects that the ion motion is limited if the ions encounter collisions. Tolmachev et al. [15] introduced an additional factor γ considering the average time τ between collisions and the period of the RF voltage determined by the angular frequency ω.

$$\gamma = \frac{\omega^2 \tau^2}{1 + \omega^2 \tau^2} \tag{2}$$

The factor γ specifies the effectiveness of the RF field suppression near the high pressure limit and reaches zero for increasing pressures. This results in the effective potential V_{eff}, which takes into account ion mass, electrode distance, and pressure dependence.

$$V_{\mathrm{eff}} = \gamma \bullet \frac{q \bullet V_{\mathrm{RF}}^2}{4 \bullet m \bullet \omega^2 \bullet \left(\frac{d}{\pi}\right)^2} = \frac{\omega^2 \tau^2}{1 + \omega^2 \tau^2} \bullet \frac{q \bullet V_{\mathrm{RF}}^2}{4 \bullet m \bullet \omega^2 \bullet \left(\frac{d}{\pi}\right)^2} \tag{3}$$

Hence, to efficiently operate an ion funnel at elevated pressures, both the RF voltage amplitude V_{RF} and the angular frequency ω have to be increased and/or the distance d between the electrodes has to be decreased to compensate the collisional damping, as shown in [18].

In addition, increasing the parasitic capacities in relation to the coupling capacitors can reduce the voltage V_{RF} coupled to the electrodes. The simplest model that can describe the reduction of the coupled voltage is the capacitive voltage divider consisting of a RF voltage source driving the coupling capacity C_{coup} and parasitic capacity C_{par} that are placed in series. The voltage provided by the amplifier is named $V_{\mathrm{RF, elec}}$. This simplified relation is given by Eq. (4). It is obvious that either large coupling capacitors are required (or the parasitic capacities need to be small).

$$V_{\mathrm{RF}} = \frac{C_{\mathrm{coup}}}{C_{\mathrm{coup}} + C_{\mathrm{par}}} \bullet V_{\mathrm{RF,elec}} \tag{4}$$

In addition to these theoretical boundaries, also technical aspects need to be considered. With large coupling capacitors, high reactive power has to be supplied especially for a large number of parallel coupling capacitors. Usually, coupling capacitors are in the range of hundreds of pF [3] up to 10 nF [26]. Therefore, the power output of the amplifier requires up to 200 W [18, 22]. With several parallel coupling capacitors, simple oscillators are hard to realize because the resulting resonance frequency is below the above-mentioned frequency range for ion funnels considering typical inductances.

Furthermore, the focusing efficiency of an ion funnel is limited to a certain mass-to-charge (m/z) range. The high

mass-to-charge ratio limit $(m/z)_{high}$ can be estimated by Eq. (5) taken from Page et al. [26]. They assume an infinite wire model for the ion funnels electrodes to calculate the cutoffs.

$$(m/z)_{high} = \frac{0.135 \cdot e \cdot V_{RF}^2}{2 \cdot m_u \cdot \omega^2 \cdot \left(\frac{d}{\pi}\right)^3 \cdot E_{DC} \cdot \sin(\alpha)} \quad (5)$$

Here, $m_u = 1.6605 \times 10^{-27}$ kg is the atomic mass unit, α is the angle of the ion funnel electrodes, e is the elementary charge, and E_{DC} is the DC voltage gradient. Conversely, Page et al. [26] found a relationship for the low mass-to-charge limit $(m/z)_{low}$.

$$(m/z)_{low} = \frac{8 \cdot e \cdot E_{DC} \cdot \sin(\alpha)}{m_u \cdot \omega^2 \cdot \frac{d}{\pi}} \quad (6)$$

Equations (5) and (6) can be explained by considering ions that try to follow the RF field: For given RF voltage amplitude V_{RF}, DC voltage gradient E_{DC}, and ion mass m, decreasing the angular frequency ω results in ions being dragged to the electrodes. In contrast, increasing the angular frequency ω leads to a reduced acceleration of ions into the center of the ion funnel due to mass inertia, as described in [27]. According to Eq. 1, the RF voltage amplitude V_{RF} affects the maximum effective potential V_{max} and thus influences the high mass-to-charge ratio limit $(m/z)_{high}$. However, unlike multipole ion guides, there is no marked dependence of the low mass-to-charge limit $(m/z)_{low}$ on the RF voltage amplitude V_{RF} [26]. Furthermore, increasing the DC voltage gradient E_{DC}, ions are accelerated to the electrodes and discharge. Thus, the DC voltage gradient E_{DC} conflicts with the focusing field, since the low mass-to-charge limit $(m/z)_{low}$ is proportional to E_{DC}. However, in PTR drift tubes and HiKE-IMS, E_{DC} must be considerably high to prevent water clustering ($E_{DC} \geq 100$ Td). Thus, to focus light energetic ions (19 u < m < 150 u), the angular frequency ω has to be increased and the angle α has to be small to decrease the low m/z limit.

The aim of this work is to design an ion funnel with RF voltage amplitudes up to 200 V at a frequency of about 5 MHz and with reduced electric DC field strengths up to 100 Td at a maximum pressure of 20 mbar being appropriate to focus light ions with high kinetic energy. Anyway, the highest effectiveness of focusing is not the aim, being able to adjust energies is more desirable for gaining flexibility in characterization and to investigate ion chemistry. Conventional ion funnels consist of a stack of narrow plate ring electrodes with decreasing inner diameter in the axial direction as visualized by Fig. 1a. The capacitors and resistors are either soldered directly to the electrodes, or the electrodes are soldered to printed circuit boards (PCB) with a network consisting of coupling capacitors and resistors [14, 19, 20] as depicted in Fig. 1 a and b. However, the maximum RF voltage amplitude applied to such electrodes is limited by the ratio between the coupling capacitance and the parasitic electrode capacitance as shown in Eq. (4). In conventional ion funnels, the parasitic capacitance can be reduced by decreasing the overlapping area of the electrodes to reach higher RF voltage amplitudes, as shown by Ibrahim [18] and Albrecht [20]. This is shown in Fig. 1b where the minimum width of the electrodes $w_{b,min}$ has been minimized compared with $w_{a,min}$ in Fig. 1a. Nonetheless, plate ring electrodes have a large overlapping area compared with planar electrodes manufactured on PCBs resulting in a fairly large parasitic capacitance considering a simple plate capacitor model. For planar electrodes manufactured on PCBs, limitations are only imposed by the design rules of the fabrication processes. Thus, the parasitic capacitance of the funnel can be significantly reduced compared with funnels build from stacked plate ring electrodes, stacked PCB ring electrodes (as shown in Fig. 1c) [23], or printed planar electrodes on a flex-PCB [28]. Following these ideas, we present a novel ion funnel that is entirely manufactured from standard PCBs with planar electrodes. Figure 1 d visualizes our ion funnel concept with reduced w_d by using planar electrodes on a PCB as already suggested by [28]. In contrast to the 3D-printed flex-PCB-based funnel of [28], our ion funnel is fabricated just using standard PCB technology to reduce costs and simplify the manufacturing process. The ion funnel just consists of six parts: four electrode PCBs including the signal distribution circuit and forming the sidewalls of the ion funnel, one PCB adapter for coupling the HiKE-IMS, and one metal adapter including the exit aperture for coupling the mass spectrometer.

Theoretical Considerations

In order to theoretically evaluate the differences between a rectangular and conical geometry of an ion funnel, numerous ion trajectory simulations have been performed using a simple model in SIMION 8.1.1.32. The size of the grid elements used in our model is 125 μm. A further decrease in the grid size was not possible due to the maximum number of elements and the width of the electrodes. To minimize the influence of discretization errors, in the simulations, ions were counted at the end of the ion funnel. This should be sufficient to compare the focusing ability of both geometries. The ion time steps are chosen as centigrade of the RF cycle time, and the electrode voltages are updated every 1 ns in order to depict the voltage progression.

In all models, neutral gas flows are neglected to visualize only the impact of geometry and adjustable voltages, assuming zero-flow air as background gas with a temperature of 20 °C. Although the ion funnel is designed to work at a pressure of 20 mbar, the first simulations will be done at a pressure of 15 mbar, because it is easier to reach the required voltages and pumping power in the later experimental validation. Collisions of ions with the background gas and diffusive movement of ions are considered by the SDS model (statistical diffusion simulation). Coulomb repulsion is neglected. According to [29], the SDS model is suitable for pressures exceeding 8 mbar.
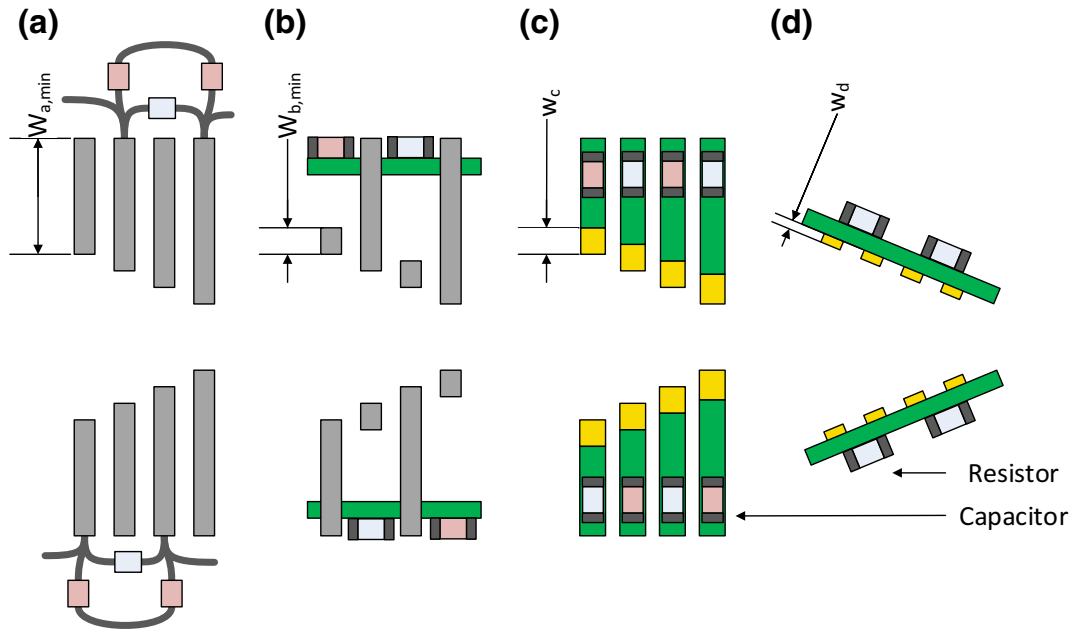
Figure 1. Different constructions of ion funnels with capacitors (red) and resistors (light gray). (**a**) Schaffer et al. [14, 19]: a stack of plate ring electrodes (gray) with wired electrical components. (**b**) Albrecht [20]: thin laser cut plate ring electrodes (gray) connected to PCBs (green) with SMD electrical components. (**c**) Chen et al. [23]: a stack of PCBs with sideplating as ring electrodes and electrical components. (**d**) Our work: PCBs with thin planar electrodes on the inside and electrical components on the outside of the ion funnel

The SDS model is based on a combination of a viscous Stokes' law drag force and a superimposed diffusion effect [24]. Ion movement is calculated by a combination of viscous ion mobility and random jumps with respect to the mean free path. In every simulation, the trajectories of 2000 ions with a mass of 19 u are calculated. All ions start uniformly distributed over a line in the cross section of the first electrode of the ion funnel. A single ion flight is terminated when it hits an electrode.

In the first step, we investigate the ion transmission of a rectangular ion funnel in comparison with a conventional conical ion funnel. Therefore, two models were compared containing 60 planar electrodes, each with a width of 500 µm and a distance of 500 µm to the next electrode, in both a rectangular and a conical geometry. In the rectangular model, the first electrode forms a 20×20 mm^2 entrance, which linearly decreases down to 2×2 mm^2. In the conical model, the inner diameter of the electrodes linearly decreases from 20 to 2 mm. For comparing both ion funnel geometries, the transmission of ions through a circular exit aperture with 2-mm inner diameter is simulated. In Fig. 2a, the transmission in dependency of the
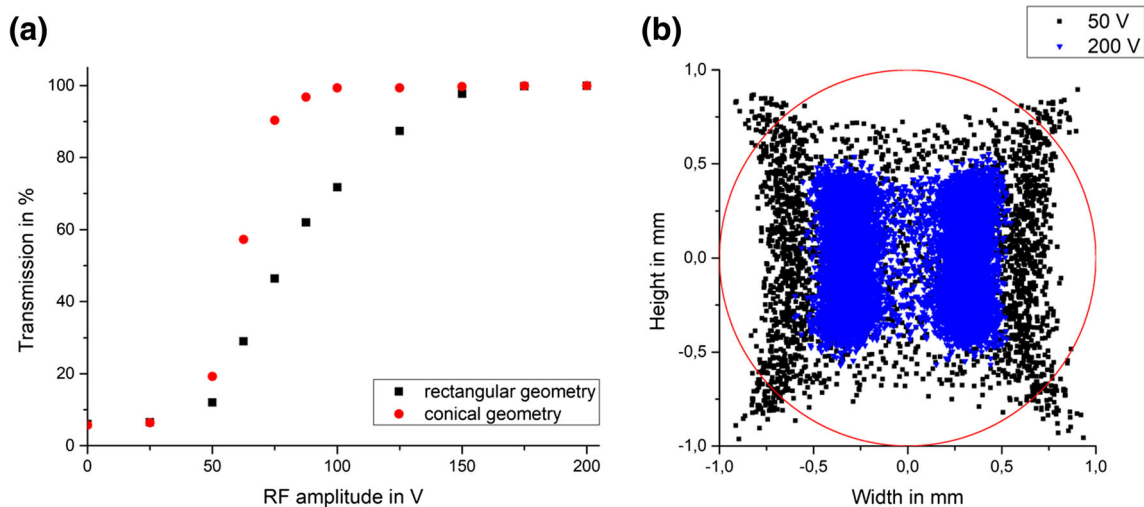

Figure 2. (**a**) Ion transmission of the rectangular and the conical ion funnel both having a circular exit aperture with 2 mm in diameter as a function of the RF voltage amplitude. The simulated ion mass is 19 u, the static reduced electric DC field strength is 30 Td, and the frequency is 4.2 MHz. (**b**) Simulated ion distribution in the plane of the exit aperture for RF voltage amplitudes of 50 V (black squares) and 200 V (blue triangles). The ion mass is 19 u, the reduced electric DC field strength is 30 Td, and the frequency is 4.2 MHz

RF voltage amplitude is shown for both geometries. A reduced electric DC field strength of 30 Td is superimposed by the RF voltage. Applying RF voltage amplitudes higher than 200 V is not possible due to the electric breakdown between the electrodes.

As known from analytical models, when increasing the RF voltage amplitude, in both models, the transmission efficiency increases until saturation is reached. However, using the rectangular geometry, slightly higher RF voltage amplitudes are required to reach maximum ion transmission. The reason is illustrated in Fig. 2b. Here, the simulated ion distribution in the plane of the circular exit aperture (red circle) behind the rectangular ion funnel is shown. The repulsive effective potential depends on the distance between ions and electrodes, leading to an ion cloud formed similar to the shape of the electrodes and thus resulting in a rectangular ion cloud at the end of the rectangular ion funnel, as depicted. Applying a high effective potential (blue triangles), all ions will pass the round exit aperture. However, at lower effective potentials (black squares), the ions on the corners of the focused ion cloud will be lost, as they do not overlap with the marked round exit apertures area. In contrast, the conical ion funnel has a last electrode of the same size and shape. Thus, few ions are lost using the conical ion funnel combined with a cylindrical exit aperture. However, increasing the RF voltage amplitude and thus increasing the repulsive effective potential, a more effective focusing of ions can be achieved even when using a rectangular geometry ion funnel.

As stated above, the aim of this work is to design an ion funnel with effective focusing of high energetic ions with low m/z ratios, such as the reactant ions, for maximum ion transmission into the mass spectrometer. Thus, the ion funnel needs to focus ions with a mass of 19 u at reduced electric DC field

strength up to 100 Td. In Fig. 3a, the effect of the reduced electric DC field strength on the ion transmission is shown. Increasing the reduced electric DC field strength results in a decreasing ion transmission for ions with a mass of 19 u due to the low m/z limit according to Eq. 6. Increasing the DC field strength leads to a shift of the low m/z limit towards higher ratios and a shift of the high m/z limit towards lower ratios, as shown in Fig. 3b. However, at a reduced electric DC field strength of 100 Td, still, 35% of all ions with a mass of 19 u are transmitted, since the m/z limit is rather soft, as described in [26]. Thus, the presented ion funnel is theoretically capable of transmitting light ions up to a large reduced electric DC field strength of 100 Td.

Ion Funnel Based on Printed Circuit Boards

As mentioned above, the presented ion funnel is entirely manufactured from standard PCBs. The PCBs used in this work are made of a glass-reinforced epoxy laminate (FR4) which is laminated with a 35-μm thin film of copper. The copper can be structured using lithographic processes to generate the necessary geometries for the electrodes with extremely high precision. Each of the four side elements of the rectangular ion funnel is equipped with sixty 500-μm-wide electrodes similar to the simulated ion funnel. These electrodes have a spacing of 500 μm, resulting in a total length of the ion funnel of 60 mm. The first electrode forms a 20×20-mm^2 entrance, which linearly decreases down to 2×2 mm^2. The exit aperture has a diameter of 0.7 mm instead of 2 mm as explained below.

The concept of the PCB ion funnel is similar to the PCB ion mobility spectrometer described in [30]. In Fig. 4b, the PCB ion
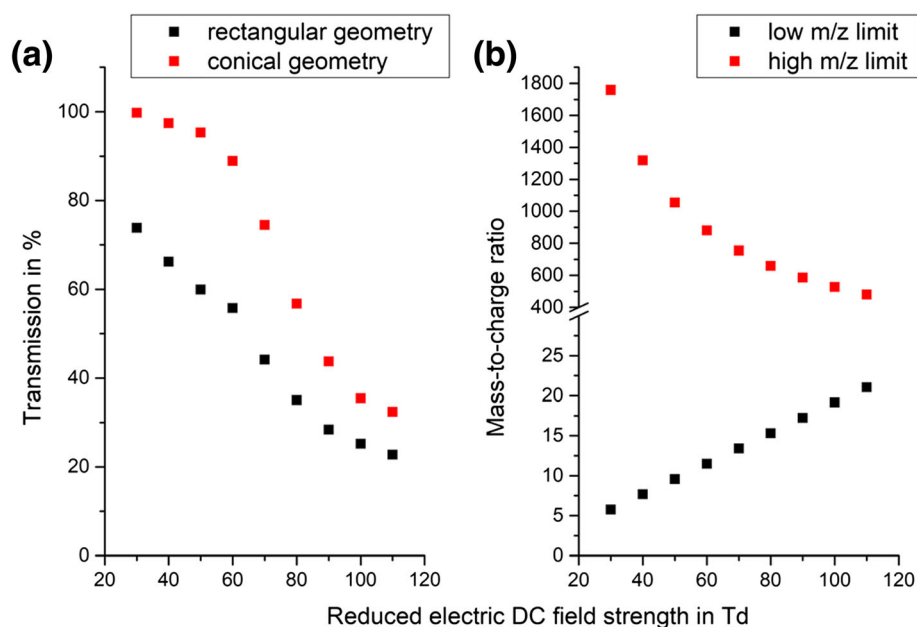

Figure 3. (a) Ion transmission in dependency of the reduced electric DC field strength for ions with mass 19 u at 100 V RF voltage amplitude and 4.2 MHz, (b) calculated low and high m/z limit according to Eqs. (5) and (6)
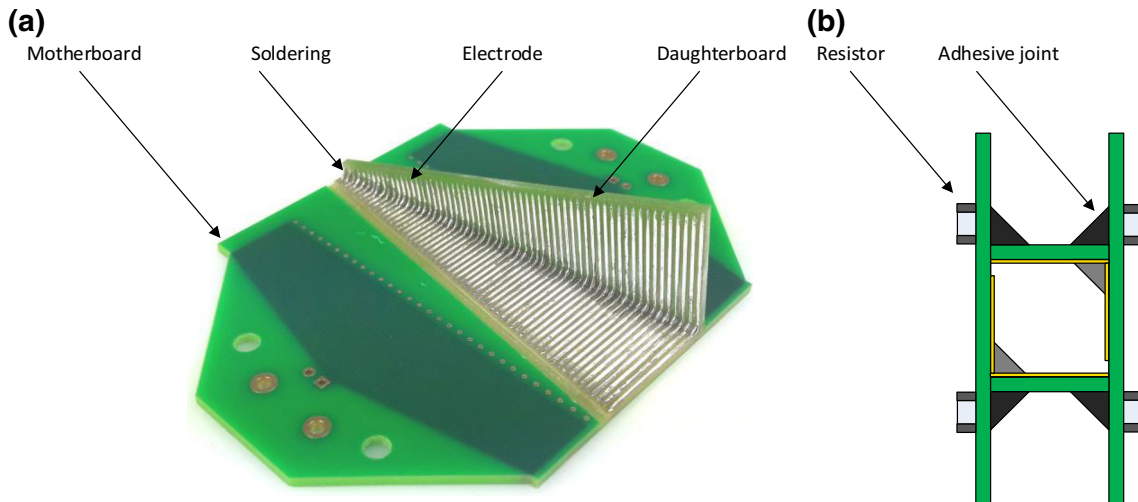
Figure 4. (**a**) A soldered half of the PCB ion funnel. (**b**) Schematic of the assembled PCB ion funnel

funnel concept is shown. Basically, the PCB ion funnel consists of four PCB parts (two motherboards and two daughterboards), which are soldered in pairs and adhered with HUNTSMAN Araldite 2014-1 forming a series of electrodes with progressively reducing the inner diameter, as depicted in Fig. 4a. The adhesive Araldite is suitable for vacuum applications (vacuum-tight and no outgassing) allowing to form a vacuum-tight chamber just by the PCBs. Thus, placing the ion funnel inside another vacuum chamber is not necessary and electrical vacuum feedthroughs are realized by the usage of sealed PCB vias. Finally, the HiKE-IMS is coupled to the ion funnel via an FR-4 adapter. The mass spectrometer is coupled via a metal adapter containing the exit aperture. Both adapters are adhered to the ion funnel using Araldite. However, the diameter of the exit aperture is 0.7 mm instead of 2 mm, in order to reduce the neutral gas flow through the ion funnel. The neutral gas flow defines the number of additional pressure stages between the ion funnel and the mass spectrometer. When the static reduced electric field strength is constant across all pressure stages, the required voltages depend on the pressures. These voltages add up to the total voltage applied to the ion funnel and increase the required dielectric strength of the ion funnel capacitors. For avoiding unrealistic high dielectric strengths, the exit aperture diameter needs to be reduced to 0.7 mm in order to have a single pressure stage between the HiKE-IMS and a future mass spectrometer. The downside is a reduced transmission of ions but a sufficient transfer of ions is still possible.

On the backside of the PCB motherboards, the electrodes are connected to the signal distribution network and via connectors to the RF and DC power supplies. The series resistor chain consists of 1% tolerance 4.99 MΩ resistors from BOURNS with a working voltage up to 400 V. This DC voltage divider provides a linear DC voltage gradient to the electrodes along the ion funnel axis. To reach high reduced electric DC field strengths of 100 Td at an elevated pressure of 20 mbar, a DC voltage gradient up to 50 V/mm is required. Two opposite in phase RF voltages are connected to adjacent electrodes via coupling capacitors. Due to the high DC voltage

gradient required for high reduced electric DC field strengths and the high RF amplitudes of up to 200 V, high dielectric strength of the coupling capacitors is necessary. As the available space on the PCB motherboards is limited, the coupling capacitors are realized as buried structures reaching 27.5–30 pF, measured with a Keysight E4990A impedance analyzer, at 5 MHz and a theoretical dielectric strength up to 6000 V. Using buried structures as capacitors is also a main difference to [28], where commercial capacitors are used. Commercial coupling capacitors will grow in size with increasing dielectric strength up to a point where connecting those to the ion funnel electrodes becomes difficult. Furthermore, coupling high RF voltage amplitudes to the electrodes requires a high ratio between the coupling capacitance and parasitic electrode capacitance as stated in Eq. (4). For comparison, conventional ion funnels with optimized stacked ring electrodes reach a parasitic capacitance of 1.6 nF [18] or 200 pF [20]. Plate ring electrodes always have a large overlapping area, while planar electrodes on PCBs with a thickness of only 35 μm lead to significantly reduced capacitance. Additionally, the parasitic capacitance is reduced by maximizing the distance between the $V_{RF, elec, +}$ and $V_{RF, elec, -}$ power lines on the PCB motherboard and using two resistor networks placed on opposite sides. The PCB ion funnel presented in this work has a measured parasitic capacitance of just 2 pF. Following Eq. (4), this would lead to a reduction of just 6 to 7% of the RF voltage V_{RF} that is coupled to the electrodes compared with the power supply voltage $V_{RF, elec}$.

The sine waveform for generating $V_{RF, elec, +}$ and $V_{RF, elec, -}$ is provided by a signal generator (RIGOL DG4062). The output of the signal generator is amplified by a 100 W RF power amplifier (Amplifier Research 100W1000A). The necessary 180° phase shift of the RF voltages is generated by using a 1:4 BalUn, which transforms the unbalanced signal oscillating relative to the ground in two balanced signals with identical amplitudes but opposite in phase. The BalUn is connected to two custom-built Hartley oscillators forming resonant circuits in combination with the coupling capacitors of the ion funnel. The resonance frequency is about 4.2 MHz.
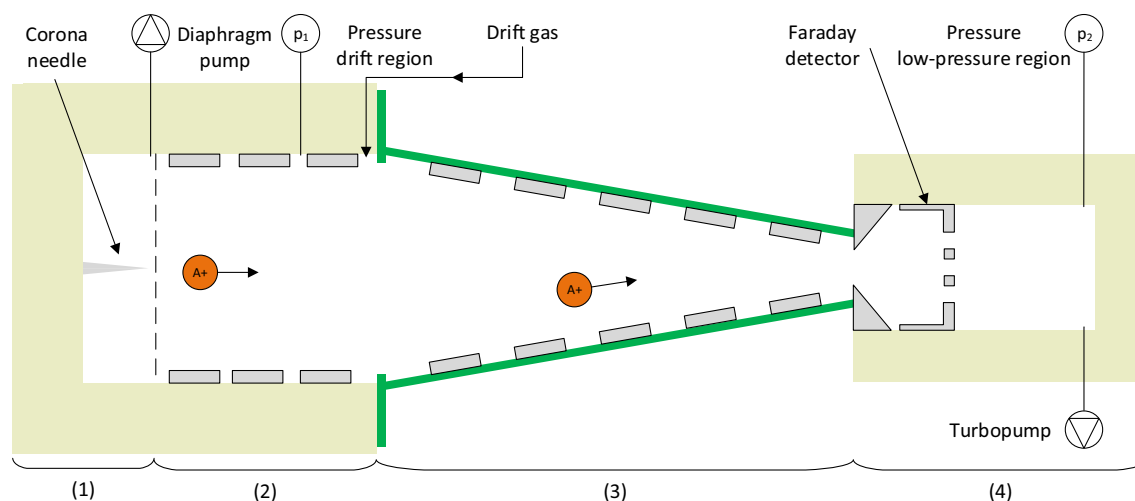
Figure 5. Experimental setup: (1) corona needle discharge; (2) drift tube; (3) ion funnel; (4) low-pressure region

Experimental Setup

In order to experimentally evaluate the ion transmission of our PCB ion funnel, the ion funnel is coupled to a HiKE-IMS, which will be assumed as a simple PTR drift tube for the test of the ion funnel operating at 15 mbar. In Fig. 5, the experimental setup is shown. It consists of four primary components: (1) a corona discharge ionization source, (2) a drift tube, (3) the ion funnel to focus ions onto the exit aperture, and (4) the low-pressure region, where on a Faraday detector behind the exit aperture of the ion funnel the transmitted ion current is measured. This is in contrast to the simulation where the ion transmission was calculated on the funnel faced side of the exit aperture. The Faraday detector is pervious to the neutral gas and connected to a current amplifier (FEMTO DLPCA-200, gain 10^9 V/A, 10 Hz). The drift tube is evacuated via a membrane pump (MVP 40, Pfeiffer Vacuum). A gas dosing valve (EVN 116, Pfeiffer Vacuum) is used to adjust the pumping rate. The pressure within the drift tube is monitored via a capacitive pressure gauge (Pfeiffer Vacuum, CMR 362). As the ion funnel is mounted directly to the drift tube, both drift tube and ion funnel are operated at the same pressure. A constant gas flow of 66 mls/min of dry clean air is led into the drift tube by a mass flow controller (Bronkhorst). The gas flow splits into two parts, one going through the ion funnel into the low-pressure region and one going towards the corona being pumped out by the diaphragm pump. The part going through the ion funnel and thus going through the pinhole into the next vacuum stage is determined by the aperture size and the pressure difference between the pressure in the ion funnel and the pressure in the next vacuum stage. A corona discharge needle (corona needle APCI, Agilent) in point-to-plane geometry is used to generate the primary ions. The drift tube consists of metallic guard rings with a constant voltage applied leading to a homogeneous electric field at a reduced electric DC field strength of 100 Td within the drift tube. Thus, the conditions are comparable to those in HiKE-IMS being operated at the same reduced electric field strength all the time. The drift tube

is coupled to the PCB ion funnel focusing the ions onto the exit aperture and transmitting the ions into a low-pressure region with 1.7×10^{-2} mbar, which is formed by a DN 40, CF 6-way cross and evacuated via a turbopump (HiPace 300, Pfeiffer Vacuum). The pressure within the low-pressure region is monitored via an active Pirani/cold cathode pressure gauge (PKR 251, Pfeiffer Vacuum).

The drift tube and the ion funnel DC voltages are provided by custom-built electronics. The output of the current amplifier is connected to a custom-built data acquisition card. The applied RF voltage amplitudes are monitored by an oscilloscope (Agilent InfiniiVision DSO-X-4104A). Table 1 gives all the operating parameters. Under such conditions, the distribution of ions generated by corona discharge ionization is shifted towards small water clusters (H_3O^+) or nitrogen oxide (NO^+) [31, 32]. Thus, ions with small masses between 19 u and 30 u enter the funnel. However, in dependency of the reduced electric DC field strength in the ion funnel, the distribution of ions might be shifted to higher masses due to clustering effects at lower reduced electric field strengths.

Table 1. Operating parameters

| Parameter	Value
Length of the drift region	269 mm
Length of ion funnel	69 mm
Drift region diameter	21 mm
Inner edge length of ion funnel (beginning)	20 mm
Inner edge length of ion funnel (end)	2 mm
RF voltage frequency	4.159 MHz
Corona voltage	1350 V
Reduced electric field in the drift region	100 Td
Reduced electric DC field in ion funnel	34–100 Td
Dew point of drift gas	−90 °C
Drift gas flow	66 ml/min
Operating pressure in the drift tube and ion funnel	15 mbar
Operating pressure in the low-pressure region	$1.7{\cdot}10^{-2}$ mbar
Operating temperature	30 °C
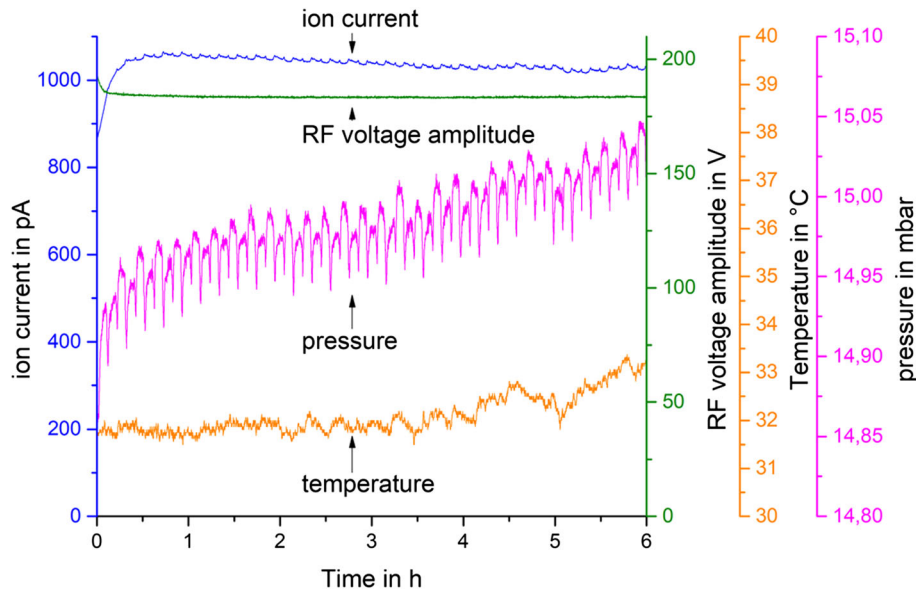
Figure 6. Ion current, RF voltage amplitude, temperature, and pressure over time after rapidly increasing the RF voltage amplitude at constant reduced electric DC field strength of 34 Td inside the ion funnel and 14.9 mbar inside the drift region and ion funnel

Results and Discussion

The ion transmission of our PCB ion funnel is investigated for different RF voltage amplitudes and reduced electric DC field strengths. Therefore, the limiting operating parameters are determined. As known from Paschen's law, the breakdown voltage is a function of gap distance and pressure. Based on Paschen's law, the theoretical breakdown voltage for air at 15 mbar and an electrode distance of 0.5 mm is 440 V. However, the breakdown voltage is additionally influenced by frequency [33]. In our ion funnel, the measured upper limit of the RF voltage amplitude is 195 V zero-to-peak at a DC voltage of 3 kV, which corresponds to a reduced electric DC field strength of 120 Td at the given pressure. These maximum possible RF voltage amplitudes and DC fields (45 V/mm) are similar to those used in a simulation by [34] with RF voltage amplitudes of 350 V zero-to-peak and electric fields up to 30 V/mm, and therefore this ion funnel could be also used as an atmospheric pressure ion funnel (APIF).

In order to investigate the dynamic behavior of the ion funnel, the ion current through the exit aperture is observed while rapidly increasing the RF voltage amplitude to 185 V (see Fig. 6). Surfaces that are not electrically conductive are prone to charging effects and might slowly be charged by ions. As can be seen in Fig. 6, it takes approximately 30 min to reach a constant ion current. However, this is due to a decrease in the RF voltage amplitude in the first 30 min caused by the self-heating of the resonant circuit. Afterwards, the pressure mainly affects the ion current. Stated in [35], the ion current is proportional to the reciprocal of the pressure, which resembles the results. A small periodic signal is visible that is caused by our zero air generator (pressure swing system). Furthermore, a small drift of the pressure can be recognized, which decreases the effective potential V_{eff} leading to a decrease in ion current.

Thus, these measurements show that the ion current is influenced by charging effects only to a small extent.

Figure 7 a shows the effect of the RF voltage amplitude on the ion current through the exit aperture. As predicted by the simulations and theoretical considerations, the ion current increases with increasing RF voltage amplitude. Figure 7 b depicts the dependency of the ion current on the reduced electric DC field. Increasing the reduced electric field strength results in a decreasing ion current. This is due to two reasons. First, as shown by the simulations in Fig. 3, the low m/z limit increases with increasing reduced electric DC field strength. Second, the ion cluster distribution changes when varying the reduced electric DC field strength [8]. Thus, with increasing reduced electric DC field strength, the ion masses decrease due to declustering effects leading to less effective focusing.

For further characterization, Fig. 8 a shows a two-dimensional sweep over the RF voltage amplitude and the reduced electric DC field. Such sweeps like this have been performed up to four times in a row 3 days. The ion current always reached the same value for the same applied voltage and reduced electric field strength again. As Fig. 8 depicts, a maximal transmitted ion current of 1060 pA for 190 V RF voltage amplitude and 34 Td at 14.9 mbar can be reached. At a reduced electric DC field strength of 100 Td, the ion current through the exit aperture is still 148 pA. The ion current is five times higher at the maximum RF voltage amplitude compared with zero RF voltage applied at maximum reduced electric DC field strength. Comparing the relative increase (five times) of the ion current at the maximum reduced electric DC field strength at 14.9 mbar to the increase (eight times) reported in [16] for protonated methanol with a mass of 33 u, our PCB ion funnel is working likewise. However, the pressure used by Barber et al. is just 1 mbar, resulting in a much higher effective potential and
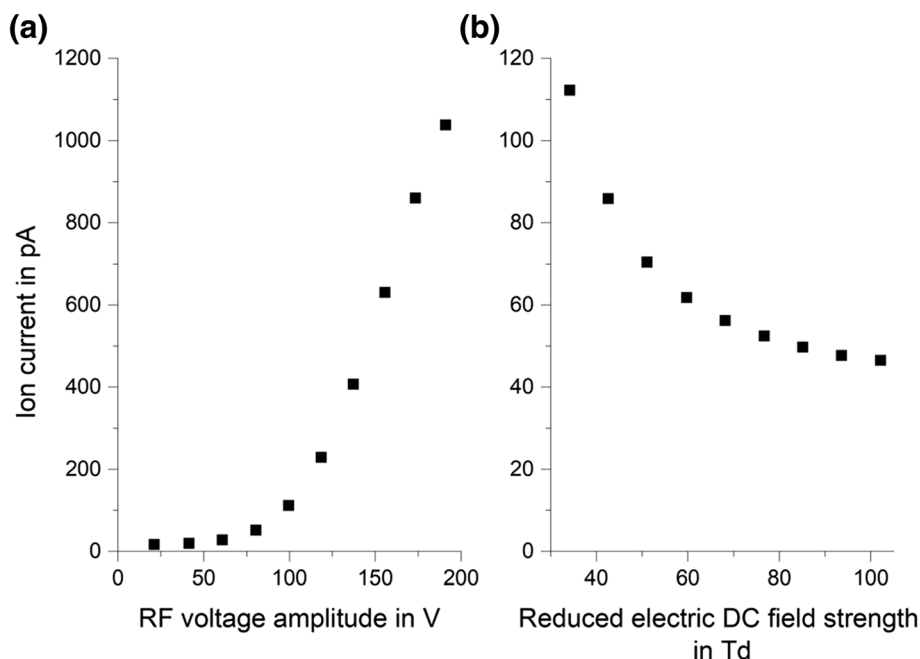
Figure 7. Transmitted ion current at a pressure of 14.9 mbar for (**a**) different RF voltage amplitudes at 34 Td reduced electric DC field strength and (**b**) different reduced electric DC field strengths at 100 V RF amplitude

easier focusing, but with only 20% higher reduced electric DC field strengths of 120 Td.

A decrease of the pressure in our ion funnel to 10 mbar also results in higher effective potentials. Here, the minimum reduced electric DC field strength is raised to 44 Td due to the minimum voltage output of the DC sources. Although the initial ion amount decreases with decreasing pressure, as shown in [35], the maximum ion current through the exit aperture can be raised to 1280 pA for 190 V RF voltage amplitude and 62 Td, as shown in Fig. 8b. At 100 Td, ion currents up to 740 pA are possible with maximum RF voltage. Again, comparing the relative increase (10 mbar 37 times) of the ion current at the maximum reduced electric DC field strength to the increase (eight times) reported in [16], our ion funnel works better. These results confirm the functionality of the ion funnel, since

the measured behavior of the ion transmission is comparable to the theoretically predicted behavior of the ion transmissions.

However, taking into account the ion current at the beginning of the ion funnel (73 nA at 100 Td and 14.9 mbar), only a maximum transmission through the exit aperture around 1.5% can be observed. This is in contrast to the simulated results predicting transmissions up to 100%. These high discrepancies can be explained mainly by two reasons: (a) the measured transmissions cannot be compared directly with the simulated data. In the simulations, ions were counted in front of the exit aperture. In the measurements, the ion current is recorded behind the exit aperture. Thus, the simulation neglects ion losses in the aperture. (b) Due to the above-mentioned issues of additional pressure stages, we plan to realize the HiKE-IMS-MS coupling with a single pressure stage between HiKE-IMS
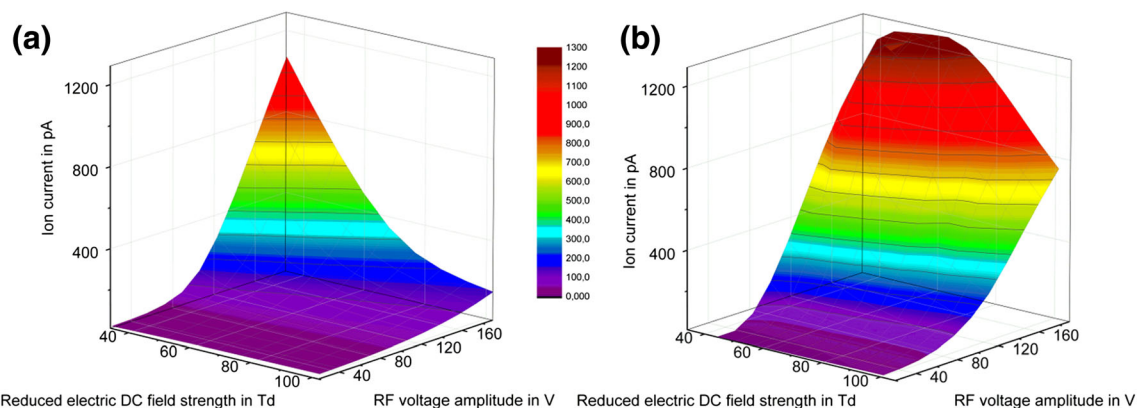

Figure 8. Surface plot of the ion current over varying reduced electric DC field strengths and RF voltage amplitudes at pressures of 14.9 mbar (**a**) and 10 mbar (**b**)

and MS. Hence, in the experimental setup, an exit aperture with 0.7 mm diameter is used instead of an exit aperture with 2 mm diameter as considered in the simulations. Due to this reduction of the aperture size, ion losses are significantly higher in the measurements. However, the focus of this work is not reaching high ion transmissions but realizing a flexible setup to investigate the ion chemistry in HiKE-IMS.

Although the total transmission is rather low, the experimental investigations proof the concept of a PCB ion funnel suitable to effectively focus ions with low m/z ratios at reduced electric DC field strengths between 30 and 100 Td. Hence, the presented approach seems to be a good compromise between parameter flexibility, manufacturing cost, RF coupling, and ion transmission.

Conclusion

In this work, we present a new ion funnel design based on standard PCB technology. By choosing PCB technology, allowing for the realization of buried structures, capacitors with very high dielectric strength and small outer dimensions can be implemented. Additionally, parasitic capacities are minimized and thus the ratio of the capacities is optimized. Considering these electrical aspects, our ion funnel outperforms other devices. The ion funnel is easy to manufacture at low cost and consists of only six parts: four electrode PCBs including the signal distribution circuit and forming the sidewalls of the ion funnel, one PCB adapter for coupling the HiKE-IMS or other drift tubes, and one metal adapter including the exit aperture for coupling a mass spectrometer. The rectangular ion funnel operates at elevated pressures between 10 and 15 mbar and effectively focuses even low weight ions. The measurement results show that our PCB ion funnel has similar performance compared with conventional ion funnels built from stacked plate ring electrodes. Furthermore, by reaching RF voltage amplitudes up to 195 V at a frequency of about 5 MHz and reduced electric DC field strengths up to 100 Td, the ion funnel is appropriate to focus light and high energetic ions. Hence, the ion funnel is suitable to couple a HiKE-IMS or other drift tubes operated at higher pressure to a mass spectrometer.

Acknowledgements

References

1. Barber, S.: Improving PTR-ToF-MS: Implementation of a Radio Frequency Ion Funnel and an Investigation into Buffer-Gas Doping. Dissertation (2015)

2. Ferreira de Brito, J.: A Lightweight High-Sensitivity Chemical Mass Spectrometer for Organic Compounds. Dissertation (2012)

3. Kirk, A.T., Grube, D., Kobelt, T., Wendt, C., Zimmermann, S.: A high resolution high kinetic energy ion mobility spectrometer based on a low-discrimination tri-state ion shutter. Anal. Chem. **90**, 5603–5611 (2018)

4. Langejuergen, J., Allers, M., Oermann, J., Kirk, A.T., Zimmermann, S.: High kinetic energy ion mobility spectrometer: quantitative analysis of gas mixtures with ion mobility spectrometry. Anal. Chem. **86**, 7023–7032 (2014)

5. Langejuergen, J., Allers, M., Oermann, J., Kirk, A.T., Zimmermann, S.: Quantitative detection of benzene in toluene- and xylene-rich atmospheres using high-kinetic-energy ion mobility spectrometry (IMS). Anal. Chem. **86**, 11841–11846 (2014)

6. Ellis, A.M., Mayhew, C.A.: Proton transfer reaction mass spectrometry: principles and applications. John Wiley & Sons, Ltd, Chichester (2014)

7. de Gouw, J.A., Goldan, P.D., Warneke, C., Kuster, W.C., Roberts, J.M., Marchewka, M., Bertman, S.B., Pszenny, A.A.P., Keene, W.C.: Validation of proton transfer reaction-mass spectrometry (PTR-MS) measurements of gas-phase organic compounds in the atmosphere during the New England Air Quality Study (NEAQS) in 2002. J. Geophys. Res. **108**, 10–1 - 10-18 (2003)

8. Gouw, J. de, Warneke, C., Karl, T., Eerdekens, G., van der Veen, Carina, Fall, R.: Sensitivity and specificity of atmospheric trace gas detection by proton-transfer-reaction mass spectrometry, Int. J. Mass Spectrom. 223-224, 365–382 (2003)

9. Eiceman, G.A., Karpas, Z., Hill, H.H.: Ion Mobility Spectrometry, 3rd edn. CRC Press, Boca Raton (2013)

10. Spangler, G.E.: Characterization of the ion-sampling pinhole interface for an ionmobility spectrometer/mass spectrometer system. J. Am. Soc. Mass Spectrom. 169–191 (2001)

11. Wei, Y.: A pulsed pinhole atmospheric pressure interface for simplified mass spectrometry instrumentation with enhanced sensitivity. Rapid Commun. Mass Spectrom. 701–706 (2015)

12. Hinterberger, F.: In: CERN (ed.) Ion Optics with Electrostatic Lenses, pp. 27–44 (2006)

13. Laughlin, B.C., Mulligan, C.C., Cooks, R.G.: Atmospheric pressure ionization in a miniature mass spectrometer. Anal. Chem. **77**, 2928–2939 (2005)

14. Shaffer, S.A., Tang, K., Anderson, G.A., Prior, D.C., Udseth, H.R., Smith, R.D.: A novel ion funnel for focusing ions at elevated pressure using electrospray ionization mass spectrometry. Rapid Commun. Mass Spectrom. **11**, 1813–1817 (1997)

15. Tolmachev, A.V., Chernushevich, I.V., Dodonov, A.F., Standing, K.G.: A collisional focusing ion guide for coupling an atmospheric pressure ion source to a mass spectrometer. Phys. Rev. B. **124**, 112–119 (1997)

16. Barber, S., Blake, R.S., White, I.R., Monks, P.S., Reich, F., Mullock, S., Ellis, A.M.: Increased sensitivity in proton transfer reaction mass spectrometry by incorporation of a radio frequency ion funnel. Anal. Chem. **84**, 5387–5391 (2012)

17. Kim, T., Udseth, H.R., Smith, R.D.: Improved ion transmission from atmospheric pressure to high vacuum using a multicapillary inlet and electrodynamic ion funnel interface. Anal. Chem. **72**, 5014–5019 (2000)

18. Ibrahim, Y., Tang, K., Tolmachev, A.V., Shvartsburg, A.A., Smith, R.D.: Improving mass spectrometer sensitivity using a high-pressure electrodynamic ion funnel interface. J. Am. Soc. Mass Spectrom. **17**, 1299–1305 (2006)

19. Kelly, R.T., Tolmachev, A.V., Page, J.S., Tang, K., Smith, R.D.: The ion funnel: theory, implementations, and applications. Mass Spectrom. Rev. **29**, 294–312 (2010)

20. Albrecht, S.: Development of a highly sensitive and versatile mass spectrometer system for laboratory and atmospheric measurements. Dissertation, Forschungszentrum Jülich, Zentralbibliothek, Jülich (2014)

21. Lynn, E.C., Chung, M.C., Han, C.C.: Characterizing the transmission properties of an ion funnel. Rapid Commun. Mass Spectrom. **14**, 2129–2134 (2000)

22. Shaffer, S.A., Tolmachev, A., Prior, D.C., Anderson, G.A., Udseth, H.R., Smith, R.D.: Characterization of an improved electrodynamic ion funnel interface for electrospray ionization mass spectrometry. Anal. Chem. **71**, 2957–2964 (1999)

23. Chen, T.-C., Webb, I.K., Prost, S.A., Harrer, M.B., Norheim, R.V., Tang, K., Ibrahim, Y.M., Smith, R.D.: Rectangular ion funnel: a new ion funnel interface for structures for lossless ion manipulations. Anal. Chem. **87**, 716–722 (2015)

24. Kim, T., Tolmachev, A.V., Harkewicz, R., Prior, D.C., Anderson, G., Udseth, H.R., Smith, R.D., Bailey, T.H., Rakov, S., Futrell, J.H.: Design and implementation of a new electrodynamic ion funnel. Anal. Chem. **72**, 2247–2255 (2000)

25. Shaffer, S.A., Prior, D.C., Anderson, G.A., Udseth, H.R., Smith, R.D.: An ion funnel interface for improved ion focusing and sensitivity using

electrospray ionization mass spectrometry. Anal. Chem. **70**, 4111–4119 (1998)

26. Page, J.S., Tolmachev, A.V., Tang, K., Smith, R.D.: Theoretical and experimental evaluation of the low *m/z* transmission of an electrodynamic ion funnel. J. Am. Soc. Mass Spectrom. **17**, 586–592 (2006)

27. Allers, M., Kirk, A.T., Zimmermann, S.: A simple centripetal force model for explaining the focusing effect of ion funnels. Int. J. Mass Spectrom. **432**, 14–17 (2018)

28. Tridas, E.M., Allemang, C., Mast, F., Anthony, J.M., Schlaf, R.: High transmission 3D printed flex-PCB-based ion funnel. J. Mass Spectrom. **50**, 938–943 (2015)

29. Anthony, D., Appelhans, D.A.D.: SIMION ion optics simulations at atmospheric pressure. Int. J. Mass Spectrom. 1–14 (2005)

30. Bohnhorst, A., Kirk, A.T., Zimmermann, S.: Simulation aided design of a low cost ion mobility spectrometer based on printed circuit boards. Int. J. Ion Mobil. Spec. **19**, 167–174 (2016)

31. Pavlik, M., Skalny, J.D.: Generation of [H3O]+.(H2O)n clusters by positive corona discharge in air. Rapid Commun. Mass Spectrom. **11**, 1757–1766 (1997)

32. Shahin, M.M.: Mass-spectrometric studies of corona discharges in air at atmospheric pressures. J. Chem. Phys. **45**, 2600–2605 (1966)

33. Sherwood Githens, J.R.: The influence of discharge chamber structure upon the initiating mechanism of the high frequency discharge. Phys. Rev. **1940**, 822–828 (1940)

34. Mayer, T., Borsdorf, H.: Ion transfer from an atmospheric pressure ion funnel into a mass spectrometer with different interface options: simulation-based optimization of ion transmission efficiency. Rapid Commun. Mass Spectrom. **30**, 372–378 (2016)

35. Kirk, A.T., Kobelt, T., Spehlbrink, H., Zimmermann, S.: A simple analytical model for predicting the detectable ion current in ion mobility spectrometry using corona discharge ionization sources. J. Am. Soc. Mass Spectrom. (2018)